ARCHIVES
of
FOUNDRY ENGINEERING

ISSN (2299-2944)
Volume 2022
Issue 2/2022

77 – 82

9/2

10.24425/afe.2022.140228

Published quarterly as the organ of the Foundry Commission of the Polish Academy of Sciences

Corrosion Behavior of FeAl and Fe_3Al Based Fe-Al-C Alloys in Sulfuric Acid

A. P. Silva *, P. P. Brito, N. Martins
PUC Minas, Brazil
* Corresponding author. E-mail address: caesilva70@hotmail.com

Received 08.11.2021; accepted in revised form 01.04.2022; available online 16.05.2022

Abstract

Iron aluminides are iron-aluminum alloys that have excellent resistance to oxidation at high temperatures with low density, high resistance/weight ratio and a low manufacturing cost. Due to its characteristics, these alloys are presented as an option to replace stainless steels in certain applications. This works intends report the casting process and subsequent analyses involving microstructure, mechanical properties, and corrosion resistance of two Fe-Al-C alloys (Fe-11wt%Al and Fe-25wt%Al, containing 0.31-0.37%C), which were prepared in an induction furnace and poured in a permanent mold. Samples of these alloys were characterized and presented elevated hardness values of 37 HRC (alloy Fe-11wt%Al) and 49.6HRC (alloy Fe-25wt%Al) and microstructure with aluminides type Fe3Al and FeAl and also carbides type K. The Fe-11wt%Al alloy exhibited superior resistance to uniform corrosion, although both Fe-Al-C alloys exhibited significantly higher corrosion rates compared to a binary iron aluminide in 0.5M H2SO4 containing naturally dissolved oxygen.

Keywords: Iron Aluminides, Microstructure, Mechanical properties, Corrosion resistance

1. Introduction

Iron aluminides are Fe-Al alloys considered to have a large potential as structural materials in severe environments due to their low density, high strength/weight ratio, elevated high temperature and corrosion and oxidation resistance as well as low manufacturing costs [1-2]. Iron aluminides can be found in ordered (FeAl, Fe_3Al) or disordered phases, and some alloys maintain ordering up to melting temperature, exhibiting elevated stability at high temperatures [3-4]. The most frequently studied iron aluminides are Fe_3Al and FeAl with approximately 20at% Al and 40at% Al, respectively, due to their good corrosion resistance and mechanical strength [3-4]. Aluminides with higher aluminum contents have low ductility at room temperature and therefore are less promising for structural applications [4]. The low ductility of iron aluminides at room temperature is attributed to hydrogen embrittlement due to reaction between aluminum and water vapor in atmosphere [5].

The improvement of mechanical properties, thermal and electrochemical behavior of binary Fe-Al intermetallics can be achieved by the addition of numerous alloying elements such as Si, V, Cr, Mn, Co, Ni, Cu, Zn, Zr, Nb and Ta. Some elements present high solubility in intermetallic (Si, V, Cr, Mn, Co, Ni, Cu, Zn) while Zr, Nb and Ta have reduced solubility. Chromium is the main alloying element added to iron aluminides [1] and is known to increase ductility because of its direct effect on hydrogen embrittlement [4]. The carbon solubility in aluminides is low at room temperature and leads to grain boundary precipitation of needle-shaped κ-type carbides. An increase in yield strength is observed with increasing the amount of carbides, but the size and distribution of these precipitates strongly influences mechanical strength. No reduction of ductility at room temperature is observed with increased carbide fraction [2].

In recent years, iron aluminide alloys have been increasingly studied concerning corrosion resistance at room temperature in aqueous media. Most investigations have focused on binary Fe-Al alloys, but given the potential for increase in mechanical strength

provided by the addition of carbon, early studies have sought to analyze the electrochemical behavior of Fe-Al-C. For instance, Rao and co-workers [6,7] and Nigam *et al*. [8] studied the influence of carbon content on the corrosion resistance of Fe-Al alloys in sulfuric acid, but so far investigations of the corrosion behavior of Fe-Al-C alloys have focused on Fe_3Al based intermetallics.

In this investigation, an analysis of the behavior in sulfuric acid of two Fe-Al-C alloys is presented, with sufficient variation in the Al-content to allow a modification of the intermetallic matrix, in order to assess the influence of the iron aluminide crystal structure on the corrosion behavior.

2. Experimental procedure

Two Fe-Al-C alloys were cast with approximately 25wt%Al and 11wt%Al, which correspond in the Fe-Al phase diagram, at room temperature, to the ordered B2 (FeAl) and $D0_3$ (Fe_3Al) structures, respectively. Preparation of the casting involved melting in an induction furnace with an alumina crucible. The material was cast in cast iron permanent molds (depicted in Figure 1), after unfavorable results were obtained after attempts in sand castings (elevated solidification times and excess porosities). From each melt, four bars with circular section were obtained (50 mm diameter and 150 mm height). Low carbon steels and aluminum alloys were used as (foundry scrap metals) as charge materials. The pouring temperatures for the Fe-25Al and Fe-11Al alloys were approximately 1668 and 1600ºC, respectively. The permanent mold used for casting was pre-heated to between 100ºC e 200ºC. The chemical composition of the cast alloys was determined by optical emission spectroscopy and is presented in Table 1.

Fig. 1. Permanent mold used for casting the iron aluminide alloys investigated in this study

The microstructure of the cast alloys was analyzed by Optical Microscopy (OM) and Scanning Electron Microscopy (SEM). Preparation for metallography involved grinding in SiC papers followed by fine polishing in a diamond suspension and etching with Villela's reagent. Grain size analysis was performed using the intercept method. Hardness measurements were performed according to the Rockwell-C method.

The corrosion behavior of the developed alloys was evaluated in a 0.5M H_2SO_4 solution containing naturally dissolved O_2. An electrochemical cell developed for flat samples was used, with an orifice of 0.78 cm^2 area for exposure to the electrolyte. The conventional three-electrode setup was employed, with an Ag/AgCl (in saturated KCl) reference electrode, Pt wire counter electrode and the sample as working electrode. The cell was connected to an IVIUM Vertex potentiostat galvanostat. The Open Circuit Potential (OCP) was initially monitored for 1.5 hours. At the stabilized OCP, Electrochemical Impedance Spectroscopy (EIS) tests were performed by applying a 10 mV sinusoidal signal within a frequency range of 100,000 to 0.01 Hz. After EIS analyses, potentiodynamic polarization scans were performed at a scan rate of 0.2 mV/s. All tests were performed at room temperature and the data was analyzed using IviumSoft software version 4.940. In order to assess the influence of carbon content on the overall corrosion resistance of the iron aluminide alloys, further electrochemical tests were performed on a binary iron aluminide alloy developed in a previous investigation [9].

Table 1.
Chemical composition (wt.%) of the alloys investigated in the present work

Alloy	Fe	Al	Mn	Si	C	Mo	P	S
Fe-25Al	74.3	24.5	0.67	0.16	0.31	0.32	0.026	0.021
Fe-11Al	87.3	10.8	0.74	0.22	0.37	0.61	0.020	0.020
Fe-15Al	85.3	14.6	-	0.003	0.003	-	0.002	0.001

3. Results and discussion

3.1. Microstructure

The microstructure of the Fe-25Al and Fe-11Al alloys is presented in Figs. 2 and 3, respectively (as revealed by OM). Coarse grains can be noticed for the two alloys (average grain diameter of 406,7μm to Fe-25Al and 322μm to Fe-11Alalloy) and presence of numerous precipitates with acicular morphology, typical of κ-type carbides dispersed in interior of grains and in grain boundaries [10]. A closer view of the κ-carbides is presented in Fig. 4. The Rockwell-C hardness of the Fe-25Al and Fe-11Al alloys were found to be, respectively 49.6 ± 2.9 and 37 ± 0.4 HRC. Given the similar carbon content and carbide distribution observed in the materials, the difference in hardness is likely caused by the different crystal structure of the two alloys.

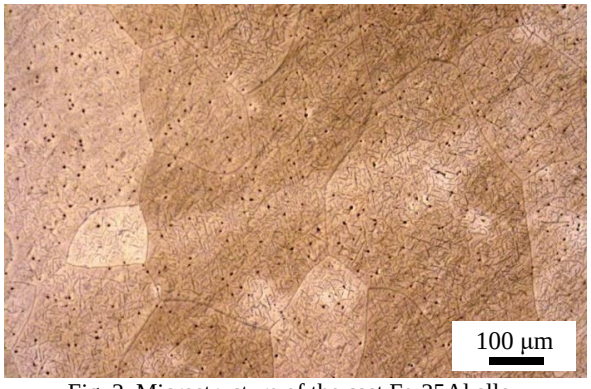

Fig. 2. Microstructure of the cast Fe-25Al alloy

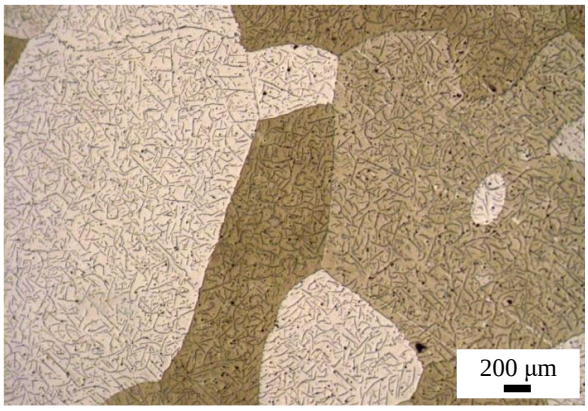

Fig. 3. Microstructure of the cast Fe-11Al alloy

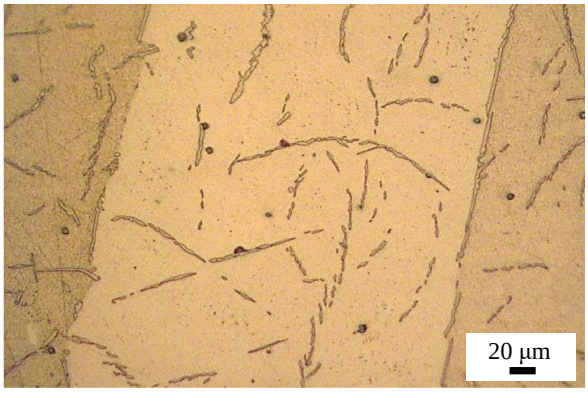

Fig. 4. Carbide morphology observed in the cast Fe-11Al alloy

3.2. Corrosion behavior

The corrosion behavior of the two Fe-Al-C alloys is analyzed in Figs. 5-7, in comparison with the binary Fe-Al alloy in the form of, polarization diagrams and EIS measurements (Nyquist plots). The equivalent circuits used to model the EIS data are shown in Fig. 8, while a summary of the electrochemical parameters that were obtained from the polarization scans and EIS measurements are presented in Tables 2 and 3, respectively.

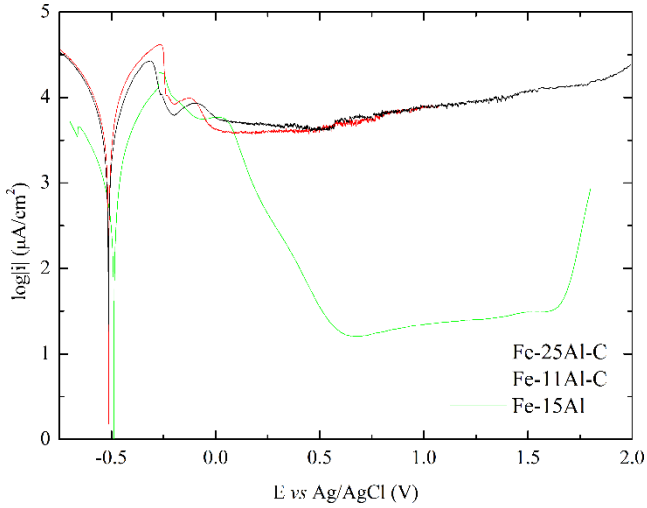

Fig. 5. Potentiodynamic polarization diagrams obtained for the Fe-25Al and Fe-11Al alloys in 0.5M H_2SO_4 containing naturally dissolved O_2

The polarization diagrams presented in Fig. 5 reveal that the three alloys exhibit an active/passive behavior, with similar values for corrosion potential (E_{corr}), as registered in Table 2. This is an indication that the Al-content and the resulting variation of crystal structure from $D0_3$ (Fe-11Al) to B2 (Fe-25Al) did not modify the anodic reaction of the freely corroding surfaces. The obtained values are consistent with previous observations concerning the corrosion behavior of iron aluminides in sulfuric acid, which yield Fe^{2+} as the main dissolved species [11] by $Fe_3Al(s) \rightarrow 3Fe^{2+}(aq) + Al(s) + 6e^-$ in case of the Fe-11Al and Fe-15Al alloys, and $FeAl(s) \rightarrow Fe^{2+}(aq) + Al(s) + 2e^-$ for the Fe-25Al alloy. The cathodic reaction is in turn given by $2H^+ + 2e^- \rightarrow H_2$. The change in Al content, however, cause variations on the actual reaction rate as evidenced by the different corrosion current density (i_{corr}) values (Table 2). The results show that Fe-25Al exhibits a lower resistance to uniform corrosion compared to the Fe-11Al alloy. The values obtained suggest similar corrosion resistance compared to previous reports concerning Fe_3Al based Fe-Al-C alloys in sulfuric acid [6], but significantly lower corrosion resistance compared to the binary Fe-Al alloy, in agreement with [12].

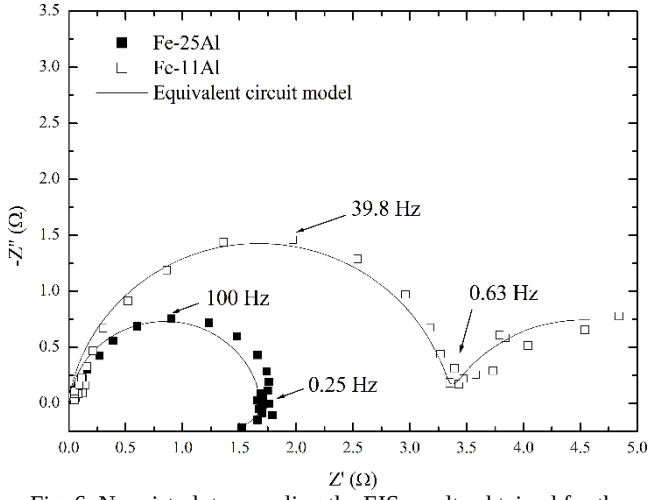

Fig. 6. Nyquist plots revealing the EIS results obtained for the cast Fe-25Al-C and Fe-11Al-C alloys

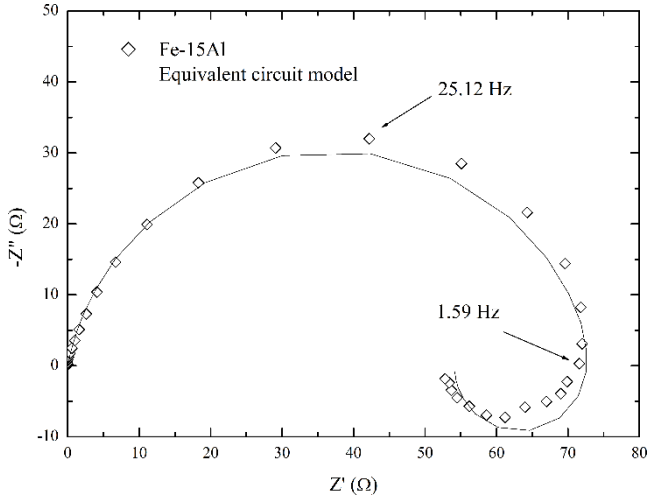

Fig. 7. Nyquist plot from Fe-15Al alloy

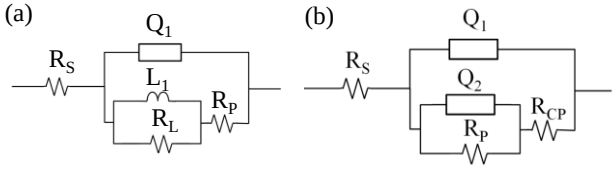

Fig. 8. Equivalent circuit models used for analyzing the EIS data: (a) Fe-25Al, Fe-15Al and (b) Fe-11Al

The higher reaction rate observed for the Fe-25Al alloy were associated with a higher critical current density (i_{crt}), indicating that a higher level of metal dissolution was observed prior to the formation of the passive layer. In other respects, however, the passive behavior of the two materials was equivalent, with similar values for the passivation potential (E_p) and passive current density (i_{pass}), as shown in Table 2. This is an indication that both materials form similar passive layers despite the differences in Al-content.

Table 2.
Summary of the potentiodynamic polarization results obtained in 0.5M H_2SO_4 containing naturally dissolved O_2 (E_{corr} – Corrosion potential; i_{corr} – corrosion current density; i_{crt} – critical current density; i_{pass} – passivation current density; E_p – passivation potential)

	E_{corr} (V)	i_{corr} (mA/cm^2)	i_{crt} (mA/cm^2)	i_{pass} (mA/cm^2)	E_p (V)
Fe-25Al	-0.52	13.5	36.6	4.16	0.02
Fe-11Al	-0.51	5.27	31.0	4.27	0.01
Fe-15Al	-0.49	1.66	3.8	0.005	0.12

Table 3.
Summary of the EIS results obtained in 0.5M H_2SO_4 containing naturally dissolved O_2 (R_s – solution resistance; R_{cp} – oxide pore resistance; R_p – polarization resistance; Q – constant phase elements; L – low frequency inductance)

	R_S (Ωcm^2)	R_p (Ωcm^2)	R_{cp} / R_L (Ωcm^2)	Q_1 (Fs^{n-1} cm^{-2})	Q_2 (Fs^{n-1} cm^{-2})	L (Hcm^2)
Fe25Al	4.67	1.27	4.15	0.0015	-	7.67
Fe11Al	6.22	3.35	2.26	0.0016	2.96	-
Fe15Al	37.0	217	79.9	3.45×10^{-5}	-	53.0

The Nyquist plots presented in Figs. 6 and 7 the presence of a depressed capacitive arc for both tested materials which were modeled by using a constant phase element (Q_1) and a polarization resistance (R_p) and two time constants. The R_p values (Table 3) obtained by equivalent circuit modeling (Fig. 8) are consistent with the results of the polarization diagrams, which revealed higher i_{corr} values on the Fe-25Al alloys. For this sample, the second time constant corresponds to an inductive element (L_1) which is usually associated with the presence of adsorbate species on the metal surface. In the present case, the adsorption layer is possibly formed by hydrogen, since the formation of H_2, as specified in the cathodic reaction, is preceded by the adsorption of hydrogen atoms on the metal surface. The same was observed for the binary Fe-Al alloy, in agreement with a previous report on the corrosion of Fe-Al single crystals [11]. For the Fe-11Al alloy, the second time constant (from a second depressed capacitive arc at lower frequencies) corresponds to a porous oxide film on the metal surface, with pore resistance R_{cp} [13]. The presence of this oxide film could indicate the reasons for the higher resistance to uniform corrosion noticed for the Fe-11Al alloy compared to the Fe-25Al alloy.

In Figure 9 the surfaces of the corroded samples (after completion of the polarization scans) are presented. The results of semi-quantitative chemical composition analysis performed by EDS are shown in Table 4. The chemical composition analysis of the corrosion layer formed on both surfaces shows the presence of oxygen, indicating the presence of oxides in the corrosion layer. The relative Fe-Al-O ratios found on the Fe-25Al and Fe-11Al alloys were $Fe_{0.77}Al_{0.15}O_{0.08}$ and $Fe_{0.43}Al_{0.14}O_{0.43}$, respectively. These values ought to be considered only semi-quantitatively, however, since EDS analysis is not accurate for predicting oxygen (or carbon) contents. In Figs. 9(a) and 9(b) it is possible to notice the presence of macro-cracks on corrosion layer formed on both samples, indicating that the passive layer formed during polarization did not completely prevent permeation from the

electrolyte and explains the relatively elevated values for passive corrosion density observed in the present study in comparison to other investigations [12].

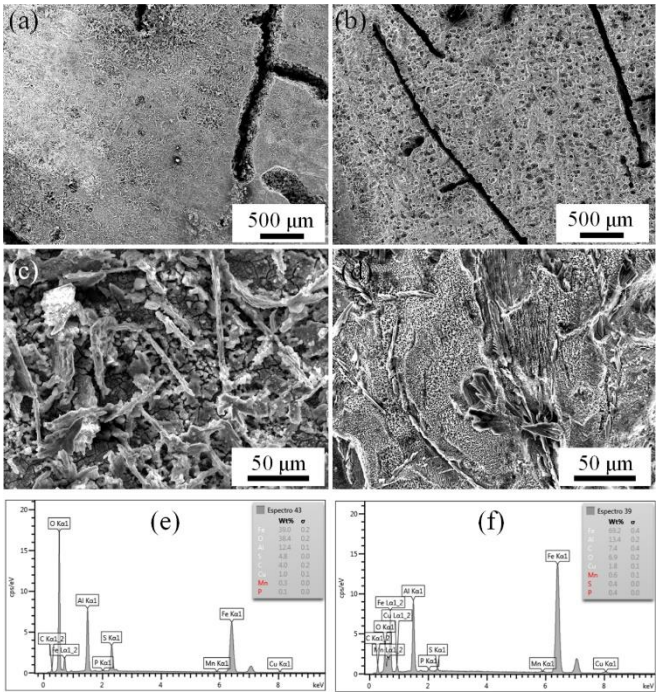

Fig. 9. Surface morphology of the corroded surfaces and EDS spectra of the Fe-25Al (a, c, e) and Fe-11Al alloy (b, d, f) after polarization measurements in 0.5M H_2SO_4 containing naturally dissolved O_2

Table 4.
Chemical composition analysis performed by EDS on the corroded metal surfaces (values in wt.%)

	Fe	Al	C	O	Cu	Mn	P	S
Fe-25Al-C	69.2	13.4	7.4	6.9	1.8	0.6	0.4	0.4
Fe-11Al-C	39.0	12.5	4.0	38.4	1.0	0.3	0.1	4.8

Observation of the oxide scales with larger magnifications, as shown in Figs. 9(c) and 9(d), revealed two distinct oxide morphologies on the corrosion layer formed on both samples: flake shaped crystals which appear as protrusions on the outer surface of the samples and an inner layer composed of equiaxed oxide crystals. In both cases, this inner oxide scale presents large quantities of defects (micro-cracks and pores).

4. Conclusions

In the present work, two Fe-Al-C alloys containing 25 and 11wt.%Al were cast and evaluated in terms of their corrosion resistance in acid medium (0.5M H_2SO_4 containing naturally dissolved O_2). The following conclusions could be drawn:

- In the as-cast condition, the materials revealed a coarse-grained microstructure with the presence secondary particles with morphology typical of κ-type carbides.
- Increasing Al-content led to an increase in hardness from 37 ± 0.4 to 49.6 ± 2.9 HRC.
- Both materials exhibited active/passive transition with similar values for corrosion potential, but slightly superior resistance to uniform corrosion for the Fe-11Al alloy.
- Contrary to the binary Fe-Al alloy, the Fe-Al-C alloys exhibited significantly higher passive current densities and corrosion rates.
- The Fe-Al-C alloys developed a porous layer of corrosion products after polarization.

Acknowledgements

The authors acknowledge financial support from FAPEMIG (PPM-00662-18) and CNPq (PQ 315533/2020-0).

References

[1] Zamanzade, M., Barnoush, A. & Motz, C. (2016). A review on the properties of iron aluminide intermetallics. *Crystals*. 6(10), 1-29. DOI: 10.3390/cryst6010010.
[2] Stoloff, N.S. (1998). Iron aluminides: present status and future prospects. *Materials Science and Engineering: A.* 258(1-2), 1-14. DOI: 10.1016/S0921-5093(98)00909-5.
[3] Cinca, N., Lima, C.R.C. & Guilemany, J.M. (2013). An overview of intermetallics research and application: Status of thermal spray coatings. *Journal of Materials Research and Technology*. 2(1), 75-86. DOI: 10.1016/j.jmrt.2013.03.013.
[4] Palm, M., Stein, F. & Dehm, G. (2019). Iron Aluminides. *Annual Review of Materials Research*. 49, 297-326. DOI: 10.1146/annurev-matsci-070218-125911.
[5] Deevi, S.C. & Sikka, V.K. (1996). Nickel and iron aluminides: an overview on properties, processing, and applications. Intermetallics. 4(5) 357-375. DOI: 10.1016/0966-9795(95)00056-9.
[6] Shankar Rao, V., Baligidad, R. G. & Raja, V. S. (2002). Effect of carbon on corrosion behaviour of Fe_3Al intermetallics in 0.5N sulphuric acid. *Corrosion Science*. 44, 521-533. DOI: 10.1016/S0010-938X(01)00084-1.
[7] Shankar Rao, V. (2005). Repassivation behaviour and surface analysis of Fe_3Al based iron aluminide in 0.25M H_2SO_4. Corrosion Science. 47, 183-194. DOI: 10.1016/j.corsci. 2004.05.014.
[8] Nigam, A.K., Balasubramaniam, R., Bhargava, S. & Baligidad, R.G. (2006). Electrochemical impedance spectroscopy and cyclic voltammetry study of carbon-alloyed iron aluminides in sulfuric acid. *Corrosion Science*. 48(7), 1666-1678. DOI: 10.1016/j.corsci.2010.05.006.
[9] Schneider, A., Falat, L., Sauthoff, G. & Frommeyer, G. (2005). Microstructures and mechanical properties of Fe3Al-based Fe-Al-C alloys. *Intermetallics*. 13(12), 1322-1331. DOI: 10.1016/j.intermet.2005.01.0.

[10] Brito, P., Pinto, H., Klaus, M., Genzel, C. & Kaysser-Pyzalla, A. (2010). Internal stresses and textures of nanostructured alumina scales growing on polycrystalline Fe_3Al alloy. *Powder Diffraction*. 25(2), 114-118. DOI: 10.1154/1.3402764
[11] Brito, P., Schuller, E., Silva, J., Campos, T.R., Araújo, C.R. & Carneiro, J.R. (2017). Electrochemical corrosion behaviour of (100), (110) and (111) Fe_3Al single crystals in sulphuric acid. *Corrosion Science*. 126, 366-373. DOI: 10.1016/j.corsci. 2017.05.029.
[12] Brito, P.P., Carvalho Filho, C.T. & Oliveira, G.A. (2020). Electrochemical corrosion behavior of iron aluminides in sulfuric acid. *Materials Science Forum*. 1012, 395-400. DOI: 10.4028/www.scientific.net/MSF.1012.395.
[13] Hernández-Hernández, M., Liu, H. B., Alvarez-Ramirez, J. & Espinosa-Medina, M. A. (2017). Corrosion behavior of Fe-40at.%Al-Based intermetallic in 0.25M H_2SO_4 solution. *Journal of Materials Engineering and Performance*. 26, 5983-5996. DOI: 10.1007/s11665-017-3036-5.